AAS 10-254

ANALYSIS OF RELATIVE GPS NAVIGATION TECHNIQUES

Matthew Fritz*, Renato Zanetti†, and Srinivas R. Vadali‡

Relative global positioning system (GPS) navigation is currently used for autonomous rendezvous and docking of two spacecraft as well as formation flying applications. GPS receivers' measurements are used by the navigation subsystem to determine estimates of the current states of the spacecraft. The success of autonomous proximity operations in the presence of an uncertain environment and noisy measurements is highly dependant on the navigation accuracy. This paper presents the comparison of four Kalman filter architectures to be used for relative GPS navigation. A trade study is performed with the advantages and disadvantages of the four different Kalman architectures used for relative GPS navigation presented and compared.

INTRODUCTION

Relative global positioning system (GPS) navigation is an area of interest currently being studied [1]. The next generation of GPS satellites known as Block IIF GPS will be launched over the next few years, paving the way for GPS navigation to be used for many years to come. Relative navigation for two spacecraft is concerned with determining estimates of both the position and velocity of one spacecraft with respect to the other [2]. Some form of GPS navigation is currently used on multiple orbiting spacecraft [1, 3–6]. With the emergence of formation flying in the past decade, multiple studies have been performed on the use GPS and differential GPS for relative spacecraft navigation for formation flying [7, 8].

The primary focus of this work is the implementation of specific Kalman filter architectures for relative GPS navigation during proximity operations involving a chaser and target vehicle. The four architectures considered for relative GPS navigation are:

1. Position Velocity (PV) Extended Kalman Filter (EKF)
2. Relative Pseudorange (RGPS) EKF
3. Pseudorange (GPS) EKF
4. Reduced GPS EKF

A GPS sensor model is used introducing various errors to the modeed pseudorange measurement [9–12]. Position and velocity estimation algorithms based on pseudorange and range rate

*Former Texas A&M Graduate Student. Member of the Technical Staff, GN&C Manned Space Systems, The Charles Stark Draper Laboratory, 17629 El Camino Real, Suite 470, Houston, Texas, 77058. mfritz@draper.com

†Senior Member of the Technical Staff, GN&C Manned Space Systems, The Charles Stark Draper Laboratory, 17629 El Camino Real, Suite 470, Houston, Texas, 77058. rzanetti@draper.com

‡Professor of Aerospace Engineering, Texas A&M University, 727B H.R. Bright Building, 3141 TAMU, College Station, TX 77843-3141. svadali@tamu.edu

measurements are implemented [13], [14]. The chaser vehicle is also assumed to have a star tracker and inertial measurement unit (IMU) located onboard. The star tracker is used to determine the orientation of the chaser vehicle. The IMU is used to determine changes in the angular velocity and translational acceleration.

With the focus on relative GPS navigation, it is expected that the RGPS and two GPS architectures will perform the best in relative state estimation while the PV architecture will perform the worst in relative state estimation. Although inertial state estimation is not the primary focus, there is a need for some inertial state information when algorithms such as Lambert targeting are used. The PV EKF and two GPS architectures are expected to perform well in inertial state estimation while the RGPS EKF is expected to perform the worst. Each architecture makes use of a dual-inertial filter where relative information is determined as the difference of the two inertial state estimates.

In this paper, models for the mentioned measurements are briefly presented, the four architectures are then introduced. Analysis of each architectures performance in relative GPS navigation is performed and advantages and disadvantages of each architectures used for relative GPS navigation are drawn through a comparison of sample covariances determined from 100 Monte Carlo runs. A single trajectory is considered for a rendezvous of a chaser vehicle with the International Space Station (ISS).

MEASUREMENT MODELS

This section presents the models of the measurements employed in the simulation. The analysis is done on the open loop navigation system. The trajectory is provided externally and consists of two altitude adjusts and four primary burns.

GPS Sensor

The GPS sensor provides the user with pseudorange measurements as well as an estimated position and velocity of the current location of the receiver based upon the pseudorange measurements. The pseudorange is defined as the distance between a particular GPS satellite at the time of signal transmission and the GPS receiver at the time of signal reception. There are six primary sources of error that affect the calculation of the pseudorange: ionosphere, troposphere, receiver clock noise, GPS satellite clock bias, multipath and ephemeris. Ionosphere, troposphere and multipath errors are all the result of time delays and therefore are always positive. Receiver clock noise, GPS satellite clock bias and ephemeris errors are due to data and clock drifting resulting in both positive and negative values. In addition to these six error sources, there is also a bias in the onboard clock of the GPS receiver. The measured pseudorange is modeled by the following equation [12]:

$$\rho_i = \|\mathbf{r}_{rec} - (\mathbf{r}_{gps_i} + \boldsymbol{\epsilon}_{eph_i})\| + \mathrm{c}(\epsilon_{iono_i} + \epsilon_{trop_i} + \epsilon_{mult_i} + \epsilon_{rcb} + \epsilon_{scb_i}) + \epsilon_\eta \tag{1}$$

$\mathbf{r}_{rec}$: position of receiver at time of signal reception (m)
$\mathbf{r}_{gps_i}$: position of the ithGPS satellite at time of signal transmission (m)
c : speed of light $= 2.99792458 \cdot 10^8 \ \frac{\text{m}}{\text{s}}$
ϵ_{iono_i} : error due to ionosphere time delay of the ithGPS satellite (s)
ϵ_{trop_i} : error due to troposphere time delay of the ithGPS satellite (s)
ϵ_{mult_i} : error due to multipath time delay of the ithGPS satellite (s)
ϵ_{rcb} : error due to receiver clock bias (s)
ϵ_{scb_i} : error due to GPS satellite clock bias of the ithGPS satellite (s)
$\boldsymbol{\epsilon}_{eph_i}$: error due to ephemeris data variations of the ithGPS satellite (m)
ϵ_{η} : error due to receiver clock noise (m)

The receiver clock bias is modeled using a second order random walk [9]. The ionosphere time delay is modeled using the Klobuchar Ionosphere model [16]. With the current altitude and orientation of the GPS receivers, the troposphere time delay is assumed to be zero for the current application. The ephemeris error is modeled as a second order Gauss-Markov process. The multipath, satellite clock bias, and receiver clock bias are modeled as first order Gauss-Markov processes. Table 1 gives the statistical information used for each Gauss-Markov model pertaining to each error source.

Active Error Sources	Steady State Standard Deviation (m)	Time Constant (s)
Ephemeris	$1\text{e}^{-3} \begin{bmatrix} 0.3748 \\ 0.5271 \\ 0.1407 \end{bmatrix}$	1800
Receiver Noise	0.7	0.1
Satellite Clock	1.8	1800
Multipath	Chaser: 0.5 Target: 2.0	200

Table 1. Gauss-Markov Error Statistics

The total pseudorange error is modeled following References [9–12]. The multipath error on the target vehicle is modeled to be slightly higher. Table 2 shows the error values used in the simulation as well as the expected values from the literature. It is assumed that only code pseudorange is used, carrier-phase and integer cycle ambiguity estimation are not used to improve the measurement.

Active Error Sources	Expected Error References [9–12]	Chaser Sensor Error (Simulation)	Target Sensor Error (Simulation)
Ionosphere	2.0-15.0	6.9	7.2
Troposphere	0.0-1.0	0.0	0.0
Ephemeris	2.0-2.5	2.1	2.1
Receiver Noise	0.0-0.7	0.7	0.7
Satellite Clock	1.0-2.0	1.8	1.8
Multipath	0.0-1.0	0.5	2.0
Total Error (RMS)	3.0-15.4	7.3	8.7

Table 2. Pseudorange Errors

Star Tracker

The star tracker is assumed to provide the attitude quaternion parametrization of the rotation from the inertial frame i to the star tracker sensor frame st. The measurement model is given as follows

$$\bar{\mathbf{q}}_i^{st} = \bar{\mathbf{q}}_b^{st} \otimes \bar{\mathbf{q}}_{error} \otimes \bar{\mathbf{q}}_i^b \otimes \bar{\mathbf{q}}_\eta \tag{2}$$

where

$\bar{\mathbf{q}}_i^{st}$: inertial to star tracker quaternion
$\bar{\mathbf{q}}_b^{st}$: body to star tracker quaternion
$\bar{\mathbf{q}}_{error}$: quaternion derived from alignment error
$\bar{\mathbf{q}}_i^b$: inertial to body quaternion
$\bar{\mathbf{q}}_\eta$: quaternion derived from tracker noise and bias, random walk

The matrix that transforms one frame to another frame, derived from Euler parameters (quaternions) relating the two frames, is given by Equation 3 [17].

$$\mathbf{T}(\bar{\mathbf{q}}\,) = I_{3\times 3} - 2q_0[\mathbf{q}_v\times] + 2[\mathbf{q}_v\times]^2 \tag{3}$$

The values for the star tracker errors are given in Table 3.

Error Type	1σ Values	Units
$\bar{\mathbf{q}}_{error}$	0.1	deg
$\bar{\mathbf{q}}_\eta$	0.0002	rad

Table 3. Star Tracker Errors

Gyroscopes

The rate gyroscopes on-board the spacecraft measure the integrated angular velocity of the vehicle. Three-axis gyroscopes are used. The mathematical model used to describe the rate gyroscopes mounted on-board the spacecraft is given by Equation 4 [18].

$$\boldsymbol{\Delta\theta}^b = \int_t^{t+\Delta t} \left\{ \boldsymbol{\omega}^b + \boldsymbol{\eta}_v + \mathbf{w}_{m_v} \right\} d\tau \tag{4}$$

$$\boldsymbol{\omega}^b = [\mathbf{T}_i^b(\bar{\mathbf{q}}_i^b)]\, \boldsymbol{\omega}^i \tag{5}$$

where

$\boldsymbol{\Delta\theta}^b$	:	change in angle vector given in body coordinate system
$\boldsymbol{\omega}^b$	:	angular velocity vector in body coordinate system
$\mathbf{T}_\mathbf{i}^\mathbf{b}$	:	transformation matrix from inertial to body coordinate system
$\boldsymbol{\eta}_v$	:	noise and bias vector associated with angular velocity, random walk
$\mathbf{w}_{m_v}$	:	first-order Markov process vector associated with angular velocity

The sample time, Δt, is 0.1 seconds. Table 4 gives the error parameters present on the gyroscopes of the IMU [19], [20].

Parameters	1σValues	Units
$\sigma_{IMU_{mis}}$	0.05	deg
σ_{m_v}	0.3	$\frac{deg}{hr}$
τ_{m_v}	3600	sec
σ_{η_v}	0.0025	$\frac{deg}{\sqrt{hr}}$
Mean error, m_{η_v}	0.5	$\frac{deg}{hr}$

Table 4. Gyroscope Model Errors

Accelerometer

The accelerometer located on-board the spacecraft measures the change in the translational velocity. The mathematical model used to describe the accelerometer mounted on-board the spacecraft is given by Equation 6 [18].

$$\boldsymbol{\Delta}\mathbf{v}_{imu} = \int_t^{t+\Delta t} \{\mathbf{a}_{imu} + \boldsymbol{\eta}_a + \mathbf{w}_{m_a}\}\, d\tau \tag{6}$$

where

$\mathbf{a}_{imu}$	:	translational acceleration vector in IMU coordinate system
$\boldsymbol{\Delta}\mathbf{v}_{imu}$	:	change in the velocity vector in IMU coordinate system
$\boldsymbol{\eta}_a$	:	noise and bias vector associated with acceleration, random walk
$\mathbf{w}_{m_a}$	:	first-order Markov process vector associated with acceleration

The sample time, Δt, is 0.1 seconds. The error parameters present in the accelerometer of the IMU model are given in Table 5 [21].

Parameters	1σ Values	Units
$\sigma_{IMU_{mis}}$	0.05	deg
σ_{m_a}	7	μg
τ_{m_a}	3600	sec
σ_{η_a}	40	$\mu g\sqrt{s}$
Mean error, m_{η_a}	40	μg

Table 5. Accelerometer Model Error Parameters

PROPAGATION MODEL

The state model for estimated state propagation of both the chaser and target vehicles is given by

$$\dot{\hat{\mathbf{r}}} = \hat{\mathbf{v}} \tag{7}$$
$$\ddot{\hat{\mathbf{r}}} = \mathbf{g}\left(\hat{\mathbf{r}}\right) + \hat{\mathbf{a}} \tag{8}$$

The gravitational acceleration is given by $\mathbf{g}\left(\hat{\mathbf{r}}\right)$ and includes effects due to the oblateness of the Earth. The gravitational acceleration is defined as [22]:

$$\begin{aligned}
\mathbf{g1}\left(\hat{\mathbf{r}}\right) &= \mathbf{u}_r + k_1\left(1 - 5U^2\right)\mathbf{u}_r + 2k_1 U\mathbf{u}_p \\
\mathbf{g2}\left(\hat{\mathbf{r}}\right) &= \mathbf{g1}\left(\hat{\mathbf{r}}\right) + 5k_2 U\left(3 - 7U^2\right)\mathbf{u}_\mathbf{r} - 3k_2\left(1 - 5U^2\right)\mathbf{u}_p \\
\mathbf{g3}\left(\hat{\mathbf{r}}\right) &= \mathbf{g2}\left(\hat{\mathbf{r}}\right) + 3k_3\left(1 - 14U^2 + 21U^4\right)\mathbf{u}_r + 4k_3 U\left(3 - 7U^2\right)\mathbf{u}_p \\
\mathbf{g}\left(\hat{\mathbf{r}}\right) &= \frac{-\mu}{\hat{\mathbf{r}}\cdot\hat{\mathbf{r}}}\mathbf{g3}
\end{aligned}$$

where

$$\begin{aligned}
k_1 &= \frac{3}{2}J_2\left(\frac{R_e}{\hat{\mathbf{r}}\cdot\mathbf{u}_r}\right)^2 \\
k_2 &= \frac{1}{2}J_3\left(\frac{R_e}{\hat{\mathbf{r}}\cdot\mathbf{u}_r}\right)^3 \\
k_3 &= -\frac{5}{8}J_4\left(\frac{R_e}{\hat{\mathbf{r}}\cdot\mathbf{u}_r}\right)^4 \\
U &= \left(\mathbf{u}_r\cdot\mathbf{u}_p\right) \\
\mathbf{u}_r &= \frac{\hat{\mathbf{r}}}{\|\hat{\mathbf{r}}\|} \\
\mathbf{u}_p &= \left[0 \;\; 0 \;\; 1\right]^T
\end{aligned}$$

and perturbation coefficients $J_\#$ and parameters are defined as follows.

$$
\begin{array}{rcl}
J_2 & : & J_2 \text{ perturbation coefficient, } 1.08263 \times 10^{-3} \\
J_3 & : & J_3 \text{ perturbation coefficient, } -2.56 \times 10^{-6} \\
J_4 & : & J_4 \text{ perturbation coefficient, } -1.58 \times 10^{-6} \\
R_e & : & \text{radius of the Earth, } 6378.1363\ km \\
\mu & : & \text{gravitation constant}
\end{array}
$$

The estimated acceleration of the chaser vehicle during thruster firings is given by Equation 9. Equation 10 gives the acceleration each vehicle experiences due to atmospheric drag. Equation 10 is used during instances of free drift.

$$
\begin{aligned}
\hat{\mathbf{a}}_c &= \hat{\mathbf{a}}_{imu} && (9) \\
\hat{\mathbf{a}}_{c,t} &= -D_{c,t} \frac{\hat{\mathbf{v}}_{c,t}}{\|\hat{\mathbf{v}}_{c,t}\|} && (10)
\end{aligned}
$$

where

$$
\begin{array}{rcl}
D_c & : & \text{chaser atmospheric drag, } 6.2 \times 10^{-6} \frac{m}{s^2} \\
D_t & : & \text{target atmospheric drag, } 12.4 \times 10^{-6} \frac{m}{s^2}
\end{array}
$$

The state dynamics matrix for the chaser vehicle is given by Equation 11.

$$
\mathbf{F}_c = \begin{bmatrix}
\mathbf{0}_{3\times3} & \mathbf{I}_{3\times3} & \mathbf{0}_{3\times3} & \mathbf{0}_{3\times3} \\
\mathbf{J_2} & \mathbf{0}_{3\times3} & [\hat{\mathbf{a}}\times] & \mathbf{T}^i_{imu} \\
\mathbf{0}_{3\times3} & \mathbf{0}_{3\times3} & -[\widetilde{\boldsymbol{\omega}}\times] & \mathbf{0}_{3\times3} \\
\mathbf{0}_{3\times3} & \mathbf{0}_{3\times3} & \mathbf{0}_{3\times3} & \mathbf{0}_{3\times3}
\end{bmatrix} \qquad (11)
$$

The matrices $[\hat{\mathbf{a}}\times]$ and $[\widetilde{\boldsymbol{\omega}}\times]$ are the skew symmetric matrices of the estimated acceleration and measured angular velocity vectors respectively. The transformation matrix $\mathbf{T}^i_{imu}$ is derived from $\bar{\mathbf{q}}^i_{imu}$. The matrix $\mathbf{J_2}$ is given as

$$
\mathbf{J_2} = \begin{bmatrix}
\frac{-m}{r^3} + \frac{3r_x^2}{r^2}\left(\frac{m}{r^3} + \Lambda(p-1)\right) & \frac{3r_x r_y}{r^2}\left(\frac{m}{r^3} + \Lambda(p-1)\right) & \frac{3r_x r_z}{r^2}\left(\frac{m}{r^3} + \Lambda(p+4)\right) \\
\frac{3r_x r_y}{r^2}\left(\frac{m}{r^3} + \Lambda(p-1)\right) & \frac{-m}{r^3} + \frac{3r_y^2}{r^2}\left(\frac{m}{r^3} + \Lambda(p-1)\right) & \frac{3r_y r_z}{r^2}\left(\frac{m}{r^3} + \Lambda(p+4)\right) \\
\frac{3r_x r_z}{r^2}\left(\frac{m}{r^3} + \Lambda(p+4)\right) & \frac{3r_y r_z}{r^2}\left(\frac{m}{r^3} + \Lambda(p+4)\right) & -(J_2(1,1) + J_2(2,2))
\end{bmatrix}
$$

where

$$
\begin{aligned}
\Lambda &= \frac{\mu J_2 R_e^2}{r^5} \\
m &= \mu\left(1 + \frac{3J_2 R_e^2 p}{4r^2}\right) \\
p &= 2\left(1 - \frac{5r_z^2}{r^2}\right)
\end{aligned}
$$

with the perturbation coefficient J_2 and parameters definitions defined the same as above. Equation 12 gives the state matrix of the target vehicle.

$$\mathbf{F}_t = \begin{bmatrix} \mathbf{0}_{3\times3} & \mathbf{I}_{3\times3} \\ \mathbf{J_2} & \mathbf{0}_{3\times3} \end{bmatrix} \tag{12}$$

The covariance matrix $\mathbf{Q}_{x_k}$ is

$$\mathbf{Q}_{x_k} = \begin{bmatrix} \mathbf{Q}_{p_{c_k}} & \mathbf{Q}_{pv_{c_k}} & \mathbf{0}_{3\times3} & \mathbf{Q}_{p_{ct_k}} & \mathbf{Q}_{pv_{ct_k}} \\ \mathbf{Q}_{pv_{c_k}} & \mathbf{Q}_{v_{c_k}} & \mathbf{0}_{3\times3} & \mathbf{Q}_{pv_{ct_k}} & \mathbf{Q}_{v_{ct_k}} \\ \mathbf{0}_{3\times3} & \mathbf{0}_{3\times3} & \mathbf{Q}_{q_k} & \mathbf{0}_{3\times3} & \mathbf{0}_{3\times3} \\ \mathbf{Q}_{p_{ct_k}} & \mathbf{Q}_{pv_{ct_k}} & \mathbf{0}_{3\times3} & \mathbf{Q}_{p_{t_k}} & \mathbf{Q}_{pv_{t_k}} \\ \mathbf{Q}_{pv_{ct_k}} & \mathbf{Q}_{v_{ct_k}} & \mathbf{0}_{3\times3} & \mathbf{Q}_{pv_{t_k}} & \mathbf{Q}_{v_{t_k}} \end{bmatrix}$$

The definition of each individual covariance matrix in $\mathbf{Q}_{x_k}$ remains the same for all four Kalman filters studied. The individual covariance matrices are given as follows where s denotes the spacecraft [22].

$$\begin{aligned} \mathbf{Q}_{p_{s_k}} &= \frac{1}{3}\mathbf{Q}_{v_{s_k}}\Delta t^2 \\ \mathbf{Q}_{pv_{s_k}} &= \frac{1}{2}\mathbf{Q}_{v_{s_k}}\Delta t \\ \mathbf{Q}_{v_{s_k}} &= \mathbf{T}^i_{lvlh}\mathbf{Q}_{s_v}(t)\mathbf{T}^{lvlh}_i\Delta t \\ \mathbf{Q}_{\theta_k} &= \mathbf{Q}_\theta(t) \\ \mathbf{Q}_{p_{ct_k}} &= \frac{19}{20}\mathbf{Q}_{p_{s_k}} \\ \mathbf{Q}_{pv_{ct_k}} &= \frac{19}{20}\mathbf{Q}_{pv_{s_k}} \\ \mathbf{Q}_{v_{ct_k}} &= \frac{19}{20}\mathbf{Q}_{v_{s_k}} \end{aligned}$$

Table 6 gives the spectral densities corresponding to each individual covariance matrix for each Kalman filter studied where s denotes chaser or target.

Spectral Density	Value	Units
$\mathbf{Q}_{s_v}(t)$	$9 \times 10^{-6}\ \mathbf{I_3}$	$\left(\frac{m}{s^{1.5}}\right)$
$\mathbf{Q}_\theta(t)$	$1 \times 10^{-11}\ \mathbf{I_3}$	$\left(\frac{rad}{\sqrt{s}}\right)$

Table 6. Spectral Density Values for all Kalman Filters

KALMAN FILTER DEVELOPMENT

Four Kalman filter architectures are studied to determine the advantages and disadvantages of each architecture for relative GPS navigation. The four architectures employ dual inertial states

that represent position and velocity of both chaser and target vehicles. Other states include the orientation of the chaser vehicle and the accelerometer bias. The architecture is an extended Kalman filter (EKF) which is a sequential state estimator that utilizes a continuous propagation of the system dynamics and a discrete update logic. The model for the states and measurements is given by Equations 13-14.

$$\begin{aligned} \dot{\mathbf{x}}(t) &= \mathbf{f}(\mathbf{x}(t), \mathbf{u}(t), t) + \mathbf{w}(t) && (13) \\ \widetilde{\mathbf{y}}_k &= \mathbf{h}(\mathbf{x}_k) + \boldsymbol{\nu}_k && (14) \end{aligned}$$

where the vector $\mathbf{w}(t)$ is a zero mean white process. The measurement model is corrupted by a zero mean white sequence $\boldsymbol{\nu}_k$ [23]. The process noise $\mathbf{w}(t)$ and the measurement noise $\boldsymbol{\nu}_k$ are assumed to be uncorrelated to each other. The spectral density of the process noise is given by $\mathbf{Q}(t)$ while the covariance matrix corresponding to the measurement noise is given by $\mathbf{R}_k$.

$$E\left\{\mathbf{w}(t)\mathbf{w}^T(\tau)\right\} = \mathbf{Q}(t)\delta(t-\tau)$$

$$E\left\{\boldsymbol{\nu}_k\boldsymbol{\nu}_j^T\right\} = \begin{cases} \mathbf{0} & k \neq j \\ \mathbf{R}_k & k = j \end{cases}$$

where $\delta(t-\tau)$ is the Dirac delta function.

Given an initial state vector and error covariance matrix

$$\begin{aligned} \hat{\mathbf{x}}(t_0) &= \hat{\mathbf{x}}_0 \\ \mathbf{e} &= \mathbf{x} - \hat{\mathbf{x}} \\ \mathbf{P}_0 &= E\left\{\mathbf{e}_0\mathbf{e}_0^T\right\} \end{aligned}$$

the Kalman gain at a given time step, $\mathbf{K}_k$, can be computed as

$$\mathbf{K}_k = \mathbf{P}_k^- \mathbf{H}_k^T(\hat{\mathbf{x}}_k^-)[\mathbf{H}_k(\hat{\mathbf{x}}_k^-)\mathbf{P}_k^-\mathbf{H}_k^T(\hat{\mathbf{x}}_k^-) + \mathbf{R}_k]^{-1} \quad (15)$$

where

$$\mathbf{H}_k(\hat{\mathbf{x}}_k^-) \equiv \left.\frac{d\mathbf{h}}{d\mathbf{x}}\right|_{\hat{\mathbf{x}}_k^-} \quad (16)$$

The state and error covariance update is

$$\begin{aligned} \hat{\mathbf{x}}_k^+ &= \hat{\mathbf{x}}_k^- + \mathbf{K}_k[\widetilde{\mathbf{y}}_k - h(\hat{\mathbf{x}}_k^-)] && (17) \\ \mathbf{P}_k^+ &= (\mathbf{I}_{n\times n} - \mathbf{K}_k\mathbf{H}_k(\hat{\mathbf{x}}_k^-))\mathbf{P}_k^-(\mathbf{I}_{n\times n} - \mathbf{K}_k\mathbf{H}_k(\hat{\mathbf{x}}_k^-))^T + \mathbf{K}_k\mathbf{R}_k\mathbf{K}_k^T && (18) \end{aligned}$$

The states are propagated as

$$\dot{\hat{\mathbf{x}}}(t) = \mathbf{f}(\hat{\mathbf{x}}(t), \mathbf{u}(t), t) \tag{19}$$
$$\mathbf{P}_{k+1}^{-} = \mathbf{\Phi}_k \mathbf{P}_k^{+} \mathbf{\Phi}_k^T + \mathbf{Q}_k \tag{20}$$

The discrete form of error covariance propagation is used where $\mathbf{P}_{k+1}^{-}$ refers to the preupdate value of the error covariance matrix and $\mathbf{P}_k^{+}$ is the postupdate covariance matrix at the previous time step. The state transition matrix is determined solving the following differential equation

$$\dot{\mathbf{\Phi}}(t, t_k) = \mathbf{F}(t)\mathbf{\Phi}(t, t_k) \quad \mathbf{\Phi}(t_k, t_k) = \mathbf{I} \tag{21}$$

$$\mathbf{F}(\hat{\mathbf{x}}(t), t) \equiv \left. \frac{d\mathbf{f}}{d\mathbf{x}} \right|_{\hat{\mathbf{x}}(t)} \tag{22}$$

The covariance matrix $\mathbf{Q}_k$ is determined from the spectral density $\mathbf{Q}(t)$.

Position Velocity Kalman Filter

The position velocity (PV) EKF processes estimated positions and velocities of each receiver's current location provided by the GPS sensor which are corrupted by colored noise. Since the EKF development assumes zero mean white process and measurement noise, additional states are augmented to the state vector to compensate for colored measurement noise. The state and measurement vectors are given as follows.

$$\begin{aligned} \mathbf{x} &= \begin{bmatrix} \mathbf{r}_c^T & \mathbf{v}_c^T & \boldsymbol{\theta}^T & \mathbf{r}_t^T & \mathbf{v}_t^T & \boldsymbol{\xi}_{r_c}^T & \boldsymbol{\xi}_{v_c}^T & \boldsymbol{\xi}_{r_t}^T & \boldsymbol{\xi}_{v_t}^T & \mathbf{a}_b^T \end{bmatrix}^T \\ \widetilde{\mathbf{y}} &= \begin{bmatrix} \widetilde{\mathbf{r}}_c^T & \widetilde{\mathbf{v}}_c^T & \widetilde{\mathbf{r}}_t^T & \widetilde{\mathbf{v}}_t^T \end{bmatrix}^T \end{aligned}$$

The chaser's accelerometer bias is modeled as first order Gauss-Markov processes with a steady state standard deviation of 40μg and time constant τ_a of 1 hour for each axis [21]. The accelerometer bias vector is given by:

$$\mathbf{a}_b = \begin{bmatrix} a_{b_x} & a_{b_y} & a_{b_z} \end{bmatrix}^T$$

The PV filter uses a linear measurement equation.

$$\dot{\mathbf{x}}(t) = \mathbf{f}(\mathbf{x}(t), \mathbf{u}(t), t) + \mathbf{w}(t) \tag{23}$$
$$\widetilde{\mathbf{y}}_k = \mathbf{H}_k \mathbf{x}_k \tag{24}$$

where $\mathbf{w}(t)$ is the white process noise and $\mathbf{H}_k$ is the measurement sensitivity matrix. There is no white measurement noise since all the measurement error is modeled as a first order Gauss-Markov process. The measurement sensitivity matrix is:

$$\mathbf{H}_k{}' = \begin{bmatrix} \mathbf{I}_{6\times6} & \frac{d\mathbf{x}_c}{d\boldsymbol{\theta}} & \mathbf{0}_{6\times6} \\ \mathbf{0}_{6\times6} & \frac{d\mathbf{x}_t}{d\boldsymbol{\theta}} & \mathbf{I}_{6\times6} \end{bmatrix} \tag{25}$$

$$\mathbf{H}_k = \begin{bmatrix} \mathbf{H}_k{}' & \mathbf{I}_{12\times12} & \mathbf{0}_{12\times3} \end{bmatrix} \tag{26}$$

where

$$\frac{d\mathbf{x}_s}{d\boldsymbol{\theta}} = \begin{bmatrix} \frac{d\mathbf{x}_s}{d\boldsymbol{\theta}} \\ \frac{d\mathbf{x}_s}{d\boldsymbol{\theta}} \end{bmatrix} = \begin{bmatrix} [(\mathbf{T}^T(\bar{\mathbf{q}_\mathbf{s}})\mathbf{r}_{o_s})\times] \\ [(\mathbf{T}^T(\bar{\mathbf{q}_\mathbf{s}})\mathbf{v}_{o_s})\times] \end{bmatrix}$$

and $\mathbf{r}_{o_c}$, $\mathbf{r}_{o_t}$ are the position vectors corresponding to the offset of the GPS sensor from the center of gravity of the vehicle and $[\mathbf{u}\times]$ denotes the skew symmetric matrix corresponding to the vector $\mathbf{u}$.

$$\mathbf{w}(t) = \begin{bmatrix} \mathbf{w}_x(t) & \boldsymbol{\nu}(t) & \mathbf{w}_a(t) \end{bmatrix}^T \tag{27}$$

$$\boldsymbol{\xi}_k = \mathbf{0}_{12\times1} \tag{28}$$

The vector $\boldsymbol{\nu}(t)$ is a zero mean white process corresponding to the colored measurement noise states. The colored noise is modeled as a first order Gauss-Markov process for all 12 states. Table 7 gives the statistics of the Markov process corresponding to colored noise.

Vehicle	σ_{ss}, 1σ Values		Time
	Position (m)	Velocity (m/s)	Constant (s)
Chaser	20	0.3	50
Target	15	0.2	50

Table 7. Statistics for Position and Velocity Errors

The process noise spectral density is given by

$$\mathbf{Q}'(t) = \begin{bmatrix} \mathbf{Q}_x(t) & \mathbf{0}_{15\times12} & \mathbf{0}_{15\times3} \\ \mathbf{0}_{12\times15} & \mathbf{Q}_\xi(t) & \mathbf{0}_{12\times3} \\ \mathbf{0}_{3\times15} & \mathbf{0}_{3\times12} & \mathbf{Q}_a(t) \end{bmatrix}$$

where $\mathbf{Q}_x(t)$ is the spectral density corresponding to the white process noise present on the position, velocity and attitude states, $\mathbf{Q}_\xi(t)$ is the spectral density of the colored noise, and $\mathbf{Q}_a(t)$ is the spectral density corresponding to the accelerometer bias states. The spectral density corresponding to the colored noise states is

$$\mathbf{Q}_\xi(t) = \begin{bmatrix} \mathbf{Q}_{p_c}(t) & \mathbf{0}_{3\times3} & \mathbf{0}_{3\times3} & \mathbf{0}_{3\times3} \\ \mathbf{0}_{3\times3} & \mathbf{Q}_{v_c}(t) & \mathbf{0}_{3\times3} & \mathbf{0}_{3\times3} \\ \mathbf{0}_{3\times3} & \mathbf{0}_{3\times3} & \mathbf{Q}_{p_t}(t) & \mathbf{0}_{3\times3} \\ \mathbf{0}_{3\times3} & \mathbf{0}_{3\times3} & \mathbf{0}_{3\times3} & \mathbf{Q}_{v_t}(t) \end{bmatrix}$$

The first subscript defines the measurement, either position or velocity, and the second subscript defines the vehicle, either chaser or target. The spectral density corresponding to a first-order Gauss-Markov process is given by

$$\mathbf{Q}_{state}(t) = \frac{2}{\tau}\sigma_{ss}^2\mathbf{I}_{3\times 3} \tag{29}$$

The discrete form of Equation 29 is given by

$$\mathbf{Q}_k = \sigma_{ss}^2\left(1 - e^{-\frac{2\Delta t}{\tau}}\right)\mathbf{I}_{3\times 3} \tag{30}$$

The covariance of each position and velocity error as well as the accelerometer bias is found using Equation 30.

The position and velocity estimation algorithms of the GPS sensor require at least four GPS satellites visible in order to provide an estimate. If less than four a visible, no estimates are provided and the PV EKF propagates the current states only.

Relative Pseudorange Kalman Filter

The relative pseudorange (RGPS) EKF processes relative pseudorange measurements. Two additional states are modeled, the relative clock bias and clock drift (Δb, Δf). As many as six relative pseudorange measurements are processed during each update. The measurement vector is populated by relative pseudoranges, $\delta\rho$, found by differencing the chaser and target pseudoranges corresponding to the same GPS satellite with each pseudorange assumed acquired at exactly the same time. The communication time delay between the two vehicles is neglected from this analysis. The state and measurement vectors for the RGPS EKF are defined as follows.

$$\begin{aligned}\mathbf{x} &= \left[\mathbf{r}_c^T \;\; \mathbf{v}_c^T \;\; \boldsymbol{\theta}^T \;\; \mathbf{r}_t^T \;\; \mathbf{v}_t^T \;\; \Delta b \;\; \Delta f \;\; \mathbf{a}_b^T\right]^T \\ \widetilde{\mathbf{y}} &= \left[\delta\rho_i \cdots \delta\rho_n\right]^T\end{aligned}$$

The scalar n is the total number of processed pseudorange measurements. The accelerometer bias is modeled as previously described. The relative clock bias and drift are modeled by a second order random walk [12] and the covariance matrix $\mathbf{Q}_{bf_k}$ is

$$\mathbf{Q}_{bf_k} = \begin{bmatrix} 4\times 10^{-19}\Delta t + 16\pi^2\times 10^{-20}\frac{\Delta t^3}{3} & 16\pi^2\times 10^{-20}\frac{\Delta t^2}{2} \\ 16\pi^2\times 10^{-20}\frac{\Delta t^2}{2} & 16\pi^2\times 10^{-20}\Delta t \end{bmatrix}$$

Under the assumption that the bias and drift of the two receivers are uncorrelated to each other, Equation 31 gives the covariance matrix $\mathbf{Q}_{\Delta bf_k}$.

$$\mathbf{Q}_{\Delta bf_k} = \mathbf{Q}_{bf_1} + \mathbf{Q}_{bf_2} \tag{31}$$

The covariance matrix $\mathbf{Q}_k$ is

$$\mathbf{Q}_k = \begin{bmatrix} \mathbf{Q}_{x_k} & \mathbf{0}_{15\times 2} & \mathbf{0}_{15\times 3} \\ \mathbf{0}_{2\times 15} & \mathbf{Q}_{\Delta bf_k} & \mathbf{0}_{2\times 3} \\ \mathbf{0}_{3\times 15} & \mathbf{0}_{3\times 2} & \mathbf{Q}_{a_k} \end{bmatrix}$$

The covariance matrix $\mathbf{Q}_{x_k}$ corresponds to the position and velocity states of both vehicles and orientation of the chaser vehicle. The covariance matrix, $\mathbf{Q}_{\Delta bf_k}$, is defined in Equation 31 and the covariance matrix, $\mathbf{Q}_{a_k}$, corresponds to the noise on the accelerometer bias. The measurement noise covariance matrix is given as:

$$\mathbf{R}_k = 2\sigma_{\delta\rho}^2 \mathbf{I}_{n\times n}$$

where $\sigma_{\delta\rho}$ is 7 meters. The steady state standard deviation is high due to the remaining measurement noise being colored instead of white. Since the measurements are relative pseudoranges, the measurement noise covariance matrix corresponding to each pseudorange is added together hence the factor of two.

The components of the measurement sensitivity matrix, $\mathbf{H}_k$ are

$$\frac{d\delta\rho_i}{d\mathbf{r}_c} = \frac{(\mathbf{r}_{gps_i} - \mathbf{r}_c)^T}{\rho_c} \tag{32}$$

$$\frac{d\delta\rho_i}{d\mathbf{r}_t} = -\frac{(\mathbf{r}_{gps_i} - \mathbf{r}_t)^T}{\rho_t} \tag{33}$$

$$\frac{d\delta\rho_i}{d\mathbf{v}_c} = [0 \;\; 0 \;\; 0] = \frac{d\delta\rho_i}{d\mathbf{v}_t} \tag{34}$$

Line of sight vectors are defined as

$$\mathbf{l}_{c_i} = \frac{(\mathbf{r}_{gps_i} - \mathbf{r}_c)}{\rho_c} \tag{35}$$

$$\mathbf{l}_{t_i} = \frac{(\mathbf{r}_{gps_i} - \mathbf{r}_t)}{\rho_t} \tag{36}$$

The derivatives of the relative pseudorange measurements with respect to the attitude angles of the chaser vehicle involves a knowledge of the location of the GPS receiver antenna. Given the location of the GPS receiver antennas as $\mathbf{r}_{o_c}$ and $\mathbf{r}_{o_t}$, the velocities are given by:

$$\mathbf{v}_{o_c} = \boldsymbol{\omega}_c \times \mathbf{r}_{o_c}$$
$$\mathbf{v}_{o_t} = \boldsymbol{\omega}_t \times \mathbf{r}_{o_t}$$

The partial derivatives of the position and velocity of the chaser and target vehicles with respect

to the chaser attitude parameters are given by

$$\frac{d\mathbf{r}_c}{d\boldsymbol{\theta}} = [(\mathbf{T}^T(\bar{\mathbf{q}}_\mathbf{c})\mathbf{r}_{o_c})\times] \tag{37}$$

$$\frac{d\mathbf{v}_c}{d\boldsymbol{\theta}} = [(\mathbf{T}^T(\bar{\mathbf{q}}_\mathbf{c})\mathbf{v}_{o_c})\times] \tag{38}$$

$$\frac{d\mathbf{r}_t}{d\boldsymbol{\theta}} = [(\mathbf{T}^T(\bar{\mathbf{q}}_\mathbf{t})\mathbf{r}_{o_t})\times] \tag{39}$$

$$\frac{d\mathbf{v}_t}{d\boldsymbol{\theta}} = [(\mathbf{T}^T(\bar{\mathbf{q}}_\mathbf{t})\mathbf{v}_{o_t})\times] \tag{40}$$

The partial derivatives of the relative pseudorange with respect to the chaser attitude is given by

$$\frac{d\delta\rho_i}{d\boldsymbol{\theta}} = \mathbf{l}_{c_i}\frac{d\mathbf{r}_c}{d\boldsymbol{\theta}} - \mathbf{l}_{t_i}\frac{d\mathbf{r}_t}{d\boldsymbol{\theta}} \tag{41}$$

The measurement sensitivity matrix is constructed as

$$\mathbf{H}_{k_i} = \begin{bmatrix} \frac{d\delta\rho_i}{d\mathbf{r}_c} & \frac{d\delta\rho_i}{d\mathbf{v}_c} & \frac{d\delta\rho_i}{d\boldsymbol{\theta}} & \frac{d\delta\rho_i}{d\mathbf{r}_t} & \frac{d\delta\rho_i}{d\mathbf{v}_t} & 1 & \mathbf{0}_{1\times 4} \end{bmatrix} \tag{42}$$

Pseudorange Kalman Filter

The pseudorange (GPS) EKF processes up to twelve pseudorange measurements, six from the chaser and six from the target. Measured pseudoranges from common GPS satellites are processed first. If there are less than six common satellites, pseudorange measurements from non-common satellites are then processed. In cases when one or both vehicles see four or less satellites, less than twelve pseudorange measurements are processed. Ten additional states are added to the existing state vector to estimate the common pseudorange errors unique to each GPS satellite and the clock bias and drift of each vehicle. The state and measurement vectors used for the GPS EKF are given as follows.

$$\begin{aligned} \mathbf{x} &= \begin{bmatrix} \mathbf{r}_c^T & \mathbf{v}_c^T & \boldsymbol{\theta}^T & b_c & f_c & \mathbf{r}_t^T & \mathbf{v}_t^T & b_t & f_t & \mathbf{a}_b^T & \boldsymbol{\xi}_\rho^T \end{bmatrix}^T \\ \widetilde{\mathbf{y}} &= \begin{bmatrix} \rho_{c_1} & \rho_{c_2} \cdots & \rho_{c_n} & \rho_{t_1} & \rho_{t_2} & \cdots & \rho_{t_n} \end{bmatrix}^T \end{aligned}$$

The common pseudorange errors are modeled using a first order Gauss-Markov process with a steady state standard deviation, σ_{ξ_ρ}, of 6 meters and a time constant, τ_{ξ_ρ}, of 100 seconds.

The covariance matrix, $\mathbf{Q}_k$, is given as follows:

$$\mathbf{Q}_k = \begin{bmatrix} \mathbf{Q}_{c_{pv_k}} & \mathbf{0}_{6\times 3} & \mathbf{0}_{6\times 2} & \mathbf{Q}_{c/t_k} & \mathbf{0}_{6\times 2} & \mathbf{0}_{6\times 3} & \mathbf{0}_{6\times 6} \\ \mathbf{0}_{3\times 6} & \mathbf{Q}_{c_{\theta_k}} & \mathbf{0}_{3\times 2} & \mathbf{0}_{3\times 6} & \mathbf{0}_{3\times 2} & \mathbf{0}_{3\times 3} & \mathbf{0}_{3\times 6} \\ \mathbf{0}_{2\times 6} & \mathbf{0}_{2\times 3} & \mathbf{Q}_{c_{bf_k}} & \mathbf{0}_{2\times 6} & \mathbf{0}_{2\times 2} & \mathbf{0}_{2\times 3} & \mathbf{0}_{2\times 6} \\ \mathbf{Q}_{t/c_k} & \mathbf{0}_{6\times 3} & \mathbf{0}_{6\times 2} & \mathbf{Q}_{t_{pv_k}} & \mathbf{0}_{6\times 2} & \mathbf{0}_{6\times 3} & \mathbf{0}_{6\times 6} \\ \mathbf{0}_{2\times 6} & \mathbf{0}_{2\times 3} & \mathbf{0}_{2\times 2} & \mathbf{0}_{2\times 6} & \mathbf{Q}_{t_{bf_k}} & \mathbf{0}_{2\times 3} & \mathbf{0}_{2\times 6} \\ \mathbf{0}_{3\times 6} & \mathbf{0}_{3\times 3} & \mathbf{0}_{3\times 2} & \mathbf{0}_{3\times 6} & \mathbf{0}_{3\times 2} & \mathbf{Q}_{a_k} & \mathbf{0}_{3\times 6} \\ \mathbf{0}_{6\times 6} & \mathbf{0}_{6\times 3} & \mathbf{0}_{6\times 2} & \mathbf{0}_{6\times 6} & \mathbf{0}_{6\times 2} & \mathbf{0}_{6\times 3} & \mathbf{Q}_{\xi_{\rho_k}} \end{bmatrix}$$

The covariance matrix corresponding to the pseudorange error states $\mathbf{Q}_{\xi_{\rho_k}}$ is given by Equation 29. The process noise covariance matrices $\mathbf{Q}_{c_{pv_k}}$, $\mathbf{Q}_{c_{\theta_k}}$, $\mathbf{Q}_{t_{pv_k}}$, $\mathbf{Q}_{t/c_k}$, and $\mathbf{Q}_{c/t_k}$ are known. The covariance matrix corresponding to the clock bias and drift of each GPS receiver is defined as follows where s denotes the vehicle, chaser or target.

$$\mathbf{Q}_{s_{bf_k}} = \begin{bmatrix} \frac{h_0}{2}\Delta t + 2h_{-1}\Delta t^2 + \frac{2}{3}\pi^2 h_{-2}\Delta t^3 & h_{-1}\Delta t + \pi^2 h_{-2}\Delta t^2 \\ h_{-1}\Delta t + \pi^2 h_{-2}\Delta t^2 & \frac{h_0}{2\Delta t} + 4h_{-1} + \frac{8}{3}\pi^2 h_{-2}\Delta t \end{bmatrix}$$

where the coefficients $h_{\#}$ are defined as

$$\begin{aligned} h_0 &: 2 \times 10^{-19}\ (s^2) \\ h_{-1} &: 7 \times 10^{-21}\ (s) \\ h_{-2} &: 2 \times 10^{-20} \end{aligned}$$

For instances when less than six satellites are visible, the correlations between the common pseudorange errors of the missing satellites and the remaining states are removed and the steady state variance of the common pseudorange error is placed in the diagonal. The estimation error covariance matrix and estimated pseudorange error state are also restructured every time new satellites are acquired, lost or both at which point correlations are removed and the covariance of the new state is set to the steady state covariance. The pseudorange error not accounted for by the common pseudorange error is modeled as a white sequence with covariance matrix, $\mathbf{R}_k$, given as follows.

$$\begin{aligned} \mathbf{R}_{k_c} &= 15 \cdot \mathbf{I}_{n\times n}\ m^2 \\ \mathbf{R}_{k_t} &= 30 \cdot \mathbf{I}_{n\times n}\ m^2 \end{aligned}$$

Sequential processing of the pseudorange measurements is used. The measurement sensitivity matrices are given by

$$\mathbf{H}_{k_c} = \begin{bmatrix} \frac{\hat{\mathbf{r}}_c}{\rho_c(\hat{\mathbf{r}}_c)} & \mathbf{0}_{1\times 6} & 1 & \mathbf{0}_{1\times 18} \end{bmatrix} \tag{43}$$

$$\mathbf{H}_{k_c}(i+22) = 1 \tag{44}$$

$$\mathbf{H}_{k_t} = \begin{bmatrix} \mathbf{0}_{1\times 11} & \frac{\hat{\mathbf{r}}_t}{\rho_c(\hat{\mathbf{r}}_t)} & \mathbf{0}_{1\times 3} & 1 & \mathbf{0}_{1\times 10} \end{bmatrix} \tag{45}$$

$$\mathbf{H}_{k_t}(i+22) = 1 \tag{46}$$

where i is the current pseudorange measurement being processed.

Reduced Pseudorange Kalman Filter

The reduced pseudorange (GPS) EKF is similar to the GPS EKF in the measurements processed and the total number of states. However, the common pseudorange error states are considered and not estimated. The effects of the common pseudorange error states on the other states are considered but not compensated for. As a result, the reduced GPS EKF is more conservative in state estimation compared to the GPS EKF. In addition, each of the six states devoted to the common pseudorange errors are not constantly associated to the same satellite. This process reduces the complexity of the filter since avoids the bookkeeping associated with which satellites correspond to which states. The bookkeeping can be omitted since the common pseudorange error states are no longer being estimated. If the states were still being estimated, bookkeeping would be performed otherwise the filter would fail. By removing the bookkeeping from the reduced GPS filter, more conservatism is also added to the state estimation errors. The reason is that when a new satellite comes replace a previews satellite in view, the correlations are not reset, hence the error are not assumed uncorrelated, which is more conservative when those states are considered only. By considering and not estimating as well as removing the bookkeeping of the common pseudorange error states, the complexity of the Kalman filter is reduced at little cost in the means of filter performance.

The measurement vector consists of pseudoranges from as many as six satellites per receiver. The number of pseudorange measurements available during every update process will vary depending upon the number of GPS satellites in view of the receiver. Again measurements from common satellites are processed first followed by measurements unique to each receiver if needed. The state and measurement vectors are as follows.

$$\begin{aligned} \mathbf{x} &= \begin{bmatrix} \mathbf{r}_c^T & \mathbf{v}_c^T & \boldsymbol{\theta}^T & b_c & f_c & \mathbf{r}_t^T & \mathbf{v}_t^T & b_t & f_t & \mathbf{a}_b^T & \boldsymbol{\xi}_{gps}^T \end{bmatrix}^T \\ \widetilde{\mathbf{y}} &= \begin{bmatrix} \rho_{c_1} & \rho_{c_2} \cdots & \rho_{c_n} & \rho_{t_1} & \rho_{t_2} & \cdots & \rho_{t_n} \end{bmatrix}^T \end{aligned}$$

The subscript n denotes the n^{th} and final visible satellite. The covariance matrix $\mathbf{Q}_k$, corresponding to the zero mean white process noise, is the same as given for the full state GPS EKF. The measurement covariance matrix, $\mathbf{R}_k$, is given by the following equation.

$$\mathbf{R}_k = \sigma_{\rho_{ss}}^2 \mathbf{I}_{n \times n} \tag{47}$$

Sequential measurement processing is used. The steady state standard deviation, $\sigma_{\rho_{ss}}$, is 5 meters. The sensitivity matrix corresponding to measured pseudoranges from the chaser vehicle is given by Equations 43-44 while Equations 45-46 give the sensitivity matrix for pseudorange measurements from the target.

RESULTS

For each Kalman architecture studied, 100 Monte Carlo runs are performed. The sample covariance from the 100 estimation errors is calculated and compared to determine the advantages and disadvantages of using each architecture for relative GPS navigation. The sample covariances shown are the root sum square (RSS) of the three directions (x, y, z) and are 1σ values. A 75° field of view is assumed for the GPS antennas located on both the chaser and target vehicles. GPS navigation is implemented from when the chaser vehicle is approximately 25 kilometers to approximately 0.5 kilometers from the target vehicle.

Figure 1 provides a comparison of the total sample standard deviation of all four Kalman architectures for the relative position between the two vehicles. The relative position estimate provided by the PV EKF is approximately twice as large as compared to the three pseudorange architectures. The large relative position error is due to the inability of the PV EKF to determine error directionality. Since the PV architecture takes advantage of calculations performed inside the GPS sensors and processes the estimated position and velocity from the GPS sensors, it cannot determine the magnitude of error in each axis. The estimated position and velocity do not provide directly information about which satellites are used to compute the estimates, therefore leading to the inability to assign directionality to the error. Therefore, the specification of position error given for the GPS sensor is assigned to each axis resulting in conservative predicted estimation errors by the estimation error covariance. Calculations similar to those performed inside the GPS sensor can be performed inside the PV architecture to determine error directionality but doing so would nullify one main advantage of the PV EKF which is its simplicity. The relative position estimation error is also higher due to the incapability to remove common pseudorange errors.

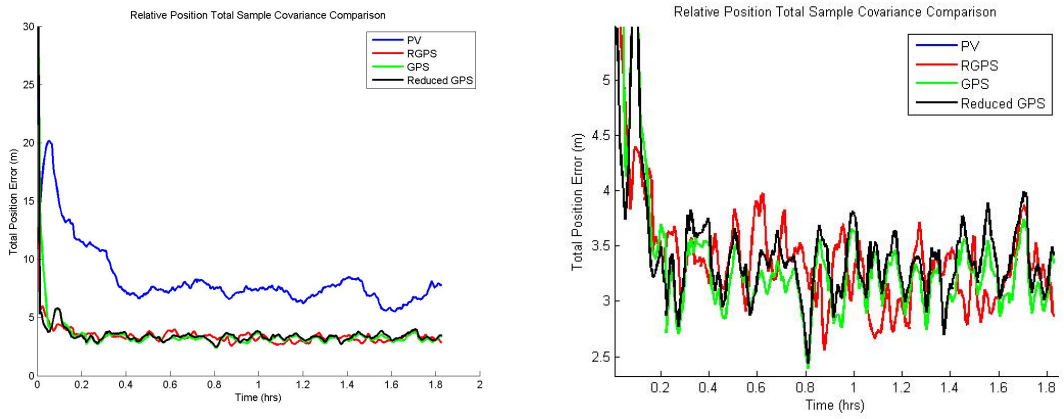

(a) Nominal (b) Zoomed

Figure 1. Relative Position RSS Sample Standard Deviation Comparison

The conservatism of the reduced GPS architecture compared to the GPS EKF is visible in Figure 1. The estimation error corresponding to the reduced GPS EKF is always slightly above the GPS EKF estimation error.

Figure 2 gives the RSS of the sample standard deviations for the four architectures corresponding to the relative velocity between the chaser and target vehicles. As is the case with the relative position error, the PV architecture again performs the worst for relative velocity estimation. Error directionality and inability to remove common pseudorange errors again result in the elevated estimation errors. In addition, the conservative nature of the reduced GPS EKF is again apparent when compared to the estimation errors for the GPS architecture. The RGPS architecture performs worse in velocity estimation compared to the two GPS architectures. The worse performance in velocity estimation is attributed to the multipath rich environment modeled. When pseudoranges from common satellites are differenced, common state errors cancel but errors due to multipath and receiver noise do not cancel. Since the multipath is relatively high on the target vehicle due to its assumed complex geometry, the remaining errors on the relative pseudoranges are higher than expected. Currently the uncommon pseudorange errors are modeled as white noise. With the re-

maining errors being colored, the filter encounters difficulty modeling the elevated colored errors as white errors. As a result, higher values are needed for the measurement covariance matrix contributing to the elevated estimation error in relative velocity. In order to achieve results comparable to the other two pseudorange architectures, additional states are required to estimate the remaining colored noise on the common pseudorange errors. However, by estimating additional states, the computational cost associated with the RGPS EKF increases therefore removing an advantage of the RGPS architecture.

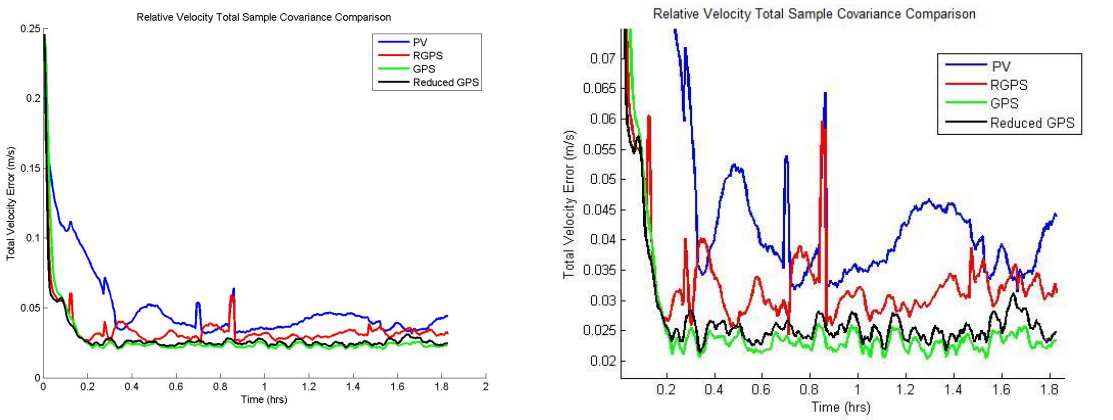

(a) Nominal (b) Zoomed

Figure 2. Relative Velocity RSS Sample Standard Deviation Comparison

CONCLUSIONS

A comparison of four different Kalman filters architectures is provided to further understand the advantages and disadvantages of using each architecture for relative GPS navigation. While the PV filter performs well in absolute state estimation, it lacks in the ability to perform as well as the pseudorange architectures in relative position and velocity estimation. The RGPS EKF is capable of providing small errors in the relative position and velocity between the two vehicle but cannot provide the user with any usable inertial state information. In addition, complications arise in the presence of multipath rich environments. The GPS EKF provides the best overall performance in both inertial and relative state estimation. However, the high complexity of the filter results in the highest computational cost of the four Kalman filters studied. The complexity and computational cost of the reduced GPS EKF are less than the GPS EKF since satellite bookkeeping is avoided and common pseudorange error states are considered instead of estimated. As a result of both the removal of the bookkeeping and common pseudorange error state consideration instead of estimation, the estimation errors are more conservative compared to those of the GPS EKF.

REFERENCES

[1] J. Gonnaud, L. Lagarde, S. Strandmoc, and A. Ballereau, "Relative GPS Navigation Implementation for the ATV Rendezvous," *Proceeding of the 5th ESA International Conference on Spacecraft Guidance, Navigation and Control Systems*, Frascati, Italy, European Space Agency, October 2002, pp. 225–232.

[2] R. Alonso, J. L. Crassidis, and J. L. Junkins, "Vision-Based Relative Navigation for Formation Flying of Spacecraft," *Proceeding of the AIAA Guidance, Navigation, and Control Conference*, Denver, CO, American Institute of Aeronautics and Astronautics, AIAA Paper #00-4439, August 2002.

[3] P. Kachmar, "Apollo and Space Shuttle On-board Navigation Systems: Application of Kalman Filtering Techniques," *Proceeding of the Institute of Navigation 58th Annual Meeting/CIGTF 21st Guidance Test Symposium*, Albuquerque, NM, American Institute of Aeronautics and Astronautics, AIAA Paper # 08-7295, June 2002, pp. 24–26.

[4] J. Gonnaud and V. Pascal, "ATV Guidance Navigation and Control for Rendezvous with ISS," *Proceeding of the 4th ESA International Conference on Spacecraft Guidance, Navigation and Control Systems*, Noordwijk, The Netherlands, European Space Agency, October 1999, pp. 501–510.

[5] K. Yamanaka, K. Yokota, K. Yamada, S. Yoshikawa, H. Koyama, K. Tsukahara, and T. Nakamura, "Guidance and Navigation System Design of R-bar Approach for Rendezvous and Docking," *Proceeding of the International Communications Satellite Systems Conference and Exhibit, 17th*, Yokohama, Japan, American Institute of Aeronautics and Astronautics, February 1998, pp. 23–27.

[6] H. Hu and T. Straube, "Orion GN&C Overview and Architecture," *Proceeding of the AIAA Guidance, Navigation and Control Conference and Exhibit*, Hilton Head, SC, American Institute of Aeronautics and Astronautics, AAS Paper #07-6678, August 2007, pp. 1–12.

[7] F. Busse and J. How, "Demonstration of Adaptive Extended Kalman Filter for Low Earth Orbit Formation Estimation using CDGPS," *NAVIGATION, Journal of The Institute of Navigation*, Vol. 50, 2003, pp. 79–94.

[8] M. L. Mitchell, "CDGPS-Based Relative Navigation for Multiple Spacecraft," Master's thesis, Massachusetts Institute of Technology, Cambridge, MA, June 2004.

[9] J. J. S. Jr., B. W. Parkinson, P. Axelrad, and P. Enge, *Global Positioning System: Theory and Application, Volume I*. Reston, VA: American Institute of Aeronautics and Astronautics, Inc., 1996.

[10] E. D. Kaplan and C. J. Hegarty, *Understanding GPS: Principles and Applications, 2nd Edition*. Norwood, MA: Artech House, Inc., 2006.

[11] B. Hofmann-Wellenhof, H. Lichtenegger, and J. Collins, *GPS Theory and Practice: Fifth, revised edition*. New York, NY: Springer-Verlag/Wien, 2001.

[12] M. S. Grewal, L. R. Weill, and A. P. Andrews, *Global Positioning Systems, Inertial Navigation, and Integration: Second Edition*. Hoboken, NJ: John Wiley & Sons, Inc., 2007.

[13] S. Bancroft, "An Algebraic Solution of the GPS Equations," *IEEE Transactions on Aerospace and Electronic Systems*, Vol. AES-21, January 1985, pp. 56–59.

[14] P. R. Escobal, *Methods of Orbit Determination*. New York, NY: John Wiley & Sons, Inc., 1965.

[15] D. Gellar, "Linear Covariance Techniques for Orbital Rendezvous Analysis and Autonomous Onboard Mission Planning," *Journal of Guidance Control and Dynamics*, Vol. 21, November-December 2006, pp. 1404–1414.

[16] J. A. Klobuchar, "Ionospheric Time-Delay Algorithm for Single-Frequency GPS Users," *IEEE Transactions on Aerospace and Electronic Systems*, Vol. 3, May 1987, pp. 325–331.

[17] H. Schaub and J. L. Junkins, *Analytical mechanics of space systems*. Reston, VA: American Institute of Aeronautics and Astronautics, Inc., 2003.

[18] W. S. F. IV, J. H. Wall, and D. M. Bevly, "Characterization of Various IMU Error Sources and the Effect on Navigation Performance," *Proceeding of the 2005 ION GNSS*, Long Beach, CA, September 13-16 2005.

[19] M. Osenar, F. Clark, and C. D'Souza, "Performance of An Automated Feature Tracking Lunar Navigation System," *Proceeding of the 31st Annual AAS Guidance and Control Conference*, Breckenridge, CO, American Astronautical Society, Paper # AAS 08-101, February 2008.

[20] "GG5300 Three Axis MEMS Rate Gyro Package," `http://www.honeywell.com/sites/servlet/com.merx.npoint.servlets.DocumentServlet?docid=D35976465-FA39-F5B2-79C1-F0FD8E49DF03`. accessed on April 23, 2009.

[21] "Q-Flex QA-3000 Accelerometer," `https://www.honeywell.com/sites/servlet/com.merx.npoint.servlets.DocumentServlet?docid=D35C68575-7711-02ED-121B-93D839D7099D`. accessed on April 23, 2009.

[22] M. H. Kaplan, *Modern Spacecraft Dynamics & Control*. Hoboken, NJ: John Wiley & Sons, Inc., 1976.

[23] J. L. Crassidis and J. L. Junkins, *Optimal Estimation of Dynamic Systems*. New York, NY: CRC Press LLC, 2004.

[24] R. Stengel, *Optimal Control and Estimation*. Mineola, NY: Dover Publications, Inc., 1994.